

Data Driven Macroscopic Modeling across Knudsen Numbers for Rarefied Gas Dynamics and Application to Rayleigh Scattering

Candi Zheng,^{*} Yang Wang,[†] and Shiyi Chen[‡]
Department of Mechanics and Aerospace Engineering
Southern University of Science and Technology,
Xueyuan Rd 1088, Shenzhen, China
Department of Mathematics
Hong Kong University of Science and Technology,
Clear Water Bay, Hong Kong SAR, China
(Dated: August 3, 2021)

Macroscopic modeling of the gas dynamics across Knudsen numbers from dense gas region to rarefied gas region remains a great challenge. The reason is macroscopic models lack accurate constitutive relations valid across different Knudsen numbers. To address this problem, we proposed a Data-driven, KnUdsen number Adaptive Linear constitutive relation model named DUAL. The DUAL model is accurate across a range of Knudsen numbers, from dense to rarefied, through learning to adapt Knudsen number change from observed data. It is consistent with the Navier-Stokes equation under the hydrodynamic limit, by utilizing a constrained neural network. In addition, it naturally satisfies the second law of thermodynamics and is robust to noisy data. We test the DUAL model on the calculation of Rayleigh scattering spectra. The DUAL model gives accurate spectra for various Knudsen numbers and is superior to traditional perturbation and moment expansion methods.

Introduction Rarefied gas dynamics are widely encountered in aerospace engineering practices such as re-entry [1], space station maintenance [2], and Lidar wind measurement [3]. Rarefied gas flow simulation is known to be difficult, due to the non-negligible dynamics corresponding to gas molecule transportation and collision at the mesoscopic scale. Simulations at the mesoscopic scale are computationally too expensive in practice, including numerically solving the Boltzmann equation [4, 5] or the Direct Simulation Monte Carlo (DSMC) [6] for flows in transition or continuous region. Coarse-grained macroscopic models could be used as a substitute to reduce the computational cost. However, they are inaccurate in describing rarefied gas flow due to a lack of accurate constitutive relations. Constitutive relations characterize mesoscopic scale dynamics as macroscopic phenomena, such as viscosity and heat conduction. Traditionally they are modeled by perturbation or expansion around the equilibrium of dense gas, such as in Hilbert and Chapman-Enskog theory [7–9] and Grad moment method [10]. As a consequence except for slightly rarefied gas flows these constitutive relation models are inaccurate. Effective ways to accurately model constitutive relations will replace expensive mesoscopic simulation and reduce the computational cost of flow simulation, hence boost its applications in industrial aerospace engineering.

Data-Driven models offer a new phenomenological approach to accurately model constitutive relations by learning from data. Such approaches have been used in related areas such as learning the governing partial dif-

ferential equation(PDE) of physical systems [11–14], simulating physical dynamics [15–17] and solving the Boltzmann equation [18]. For macroscopic modeling of rarefied gas dynamics, there have been attempts to learn a PDE for DSMC results [19] and to find correct moment equations [20]. These attempts have proven the concept of data-driven modeling and learning of the dynamics at a specific degree of rarefaction, characterized by a specific Knudsen number. However, instead of a specific Knudsen number, the ability to predict across a range of Knudsen numbers is crucial for a practical model. The only way to achieve this is to model and learn the dependency of constitutive relation across a range of Knudsen numbers, which is the focus of this letter.

To design and test models for constitutive relation, we choose the problem of calculating Rayleigh scattering spectra as our benchmark case. This problem has been well studied [21]. The accuracy of spectra depends on the correctness of the rarefied dynamics model, thus making it a good benchmark. Another advantage of this problem is its linear nature, which simplifies the possible form of constitutive relation. Still, even with the linearity it is highly nontrivial to model the dependency of constitutive relation across a range of Knudsen numbers both to satisfy the second law of thermodynamics and to ensure consistency with limiting cases.

In this letter we propose a Data-driven, knUdsen number Adaptive Linear constitutive relation model named the DUAL model. Its Knudsen number dependency is achieved by using Knudsen number adaptive viscosity. This adaptive viscosity is then approximated through a constrained neural network to make our model consistent with the Navier-Stokes equation. The second law of thermodynamics is now automatically satisfied by the nature of viscosity. Moreover, we show that this adap-

^{*} zhengcd@mail.sustech.edu.cn, czhengac@connect.ust.hk

[†] yangwang@ust.hk

[‡] chensy@sustech.edu.cn, corresponding author

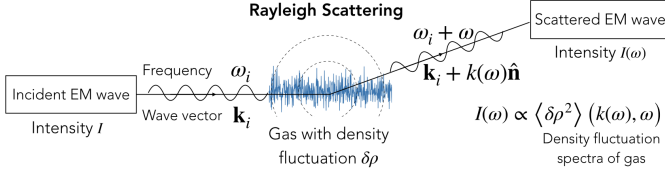


FIG. 1. Rayleigh scattering of electromagnetic(EM) waves with wave vector \mathbf{k}_i and frequency ω_i through gas with density fluctuation $\delta\rho$. $\hat{\mathbf{n}}$ is a unit vector. The intensity $I(\omega)$ of scattered EM wave with frequency shift ω is the Rayleigh scattering spectra. The Rayleigh scattering spectra are proportional to and determined by the density fluctuation spectra $\langle \delta\rho^2 \rangle$. Therefore to compute the Rayleigh scattering spectra, we need only to compute the density fluctuation spectra of gas.

tive viscosity is sufficient to model all linear constitutive relations, under the constraint of non-decreasing entropy. Finally, by avoiding derivative estimations the DUAL model is robust to noisy data. In the numerical experiment, the DUAL model is applied to calculate the Rayleigh scattering spectra and it significantly outperforms the Chapman-Enskog expansion and Grad moment methods.

Methods The *Rayleigh scattering* describes the refraction of electromagnetic waves (EM waves) passing through media with stochastic density fluctuation [22, 23]. Such fluctuation usually appears as density fluctuation waves and happens spontaneously with the thermal motion of gas molecules. The *Rayleigh scattering spectra* are defined as the intensities $I(\omega)$ of scattered EM waves after the Rayleigh scattering with frequency shifts ω , as shown in Fig 1. They are proportional to the density fluctuation spectra of gas [5, 24]

$$I(\omega) \propto \langle \delta\rho^2 \rangle(k(\omega), \omega), \quad (1)$$

where k is the wavenumber change of the scattered EM wave and $\langle \delta\rho^2 \rangle$ is the *density fluctuation spectra*, which describes the intensity of density fluctuation waves at each wavenumber k and frequency ω . Consequently to calculate the Rayleigh scattering spectra all we need is to compute the density fluctuation spectra of the gas media.

Density fluctuation spectra are closely related to the *Knudsen number*, which describes the degree of rarefaction of the gas media. It is defined as the ratio between the mean free path of gas molecules and the length scale of dynamics. For our study the length scale of dynamics is the density fluctuation wavelength. Therefore the Knudsen number in our study is given by

$$\text{Kn} = \sqrt{\frac{m}{k_B T_0}} \frac{\mu_0 k}{2\pi\rho_0}, \quad (2)$$

in which ρ_0, T_0 are the reference density and temperature, k_B is the Boltzmann constant, μ_0 is the viscosity coefficient, m is the mass of the gas molecule, and k is the density fluctuation wavenumber which is inversely

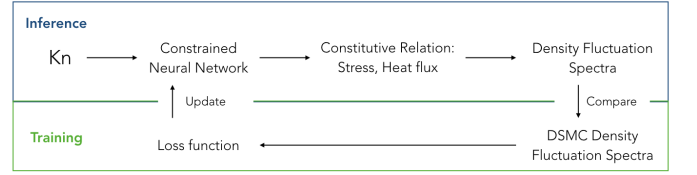


FIG. 2. The flow chart of our model to calculate the density fluctuation spectra.

proportional to wavelength. In addition, we only need to consider positive k because for k and $-k$ the spectra are the same. For Rayleigh scattering, the density fluctuation wavelength is often of the same order as the mean free path of the gas molecule. This means the Knudsen number is not negligible, and the effect of rarefied gas significantly affects the density fluctuation spectra.

To calculate the density fluctuation spectra $\langle \delta\rho^2 \rangle$, we analyze the thermodynamic fluctuation according to macroscopic governing equations. These macroscopic governing equations form a 1D linear PDE system. Its non-dimensionalized version is defined as

$$\begin{aligned} \frac{\partial\rho}{\partial t} + \frac{\partial v}{\partial x} &= 0 \\ \frac{\partial v}{\partial t} + \frac{\partial T}{\partial x} + \frac{\partial\rho}{\partial x} &= -\text{Kn} \frac{\partial\sigma}{\partial x} \\ \frac{3}{2} \frac{\partial T}{\partial t} + \frac{\partial\rho}{\partial x} &= -\frac{15}{4} \text{Kn} \frac{\partial q}{\partial x}, \end{aligned} \quad (3)$$

in which ρ, v, T are the non-dimensionalized density, velocity and temperature, respectively. Their corresponding equations represent conservation laws for mass, momentum, and energy respectively. The density fluctuation spectra $\langle \delta\rho^2 \rangle$ could be obtained from (3) by Fourier-transform after an ensemble average. However, (3) is unclosed with two extra unknown terms: the stress σ and the heat flux q that encode rarefied gas dynamics. To close (3) and solve the density fluctuation spectra, constitutive relations that model the stress and the heat flux with known quantities are necessary.

We consider the constitutive relation for the stress and heat flux as functionals. These functionals are linear because the macroscopic governing equations are linear. Our proposed DUAL model for constitutive relation functionals are in the form

$$\begin{aligned} \sigma(x) &= -\frac{\partial}{\partial x} \int \tilde{M}(x-y)v(y)dy \\ q(x) &= -\frac{\partial}{\partial x} \int \tilde{K}(x-y)T(y)dy, \end{aligned} \quad (4)$$

where \tilde{M}, \tilde{K} are convolution kernels. These kernels have certain constraints that are represented in the Fourier space as

$$\begin{aligned} \sigma(k) &= -ikM(\text{Kn})\tilde{v}_k; & M(\text{Kn}) &\geq 0 \\ q(k) &= -ikK(\text{Kn})\tilde{T}_k; & K(\text{Kn}) &\geq 0, \end{aligned} \quad (5)$$

where k is the non-dimensionalized wavenumber in the Fourier space, M, K are the spatial Fourier transforms of the kernels \tilde{M}, \tilde{K} respectively with k being replaced with the Knudsen number Kn in (2), and \tilde{v}_k, \tilde{T}_k are the spatial Fourier transform of v, T . The real functions M and K will be modeled and computed in our study via neural networks from data without the need for using derivatives. Therefore the DUAL model represents a highly robust model against noisy data. As we will discuss later, (5) ensures a non-decreasing entropy. However, it does not guarantee consistency with the Navier-Stokes equation. To address this issue, we need to constraint the neural networks modeling the real functions M, K .

The M, K modeled by neural networks should be consistent with the Navier-Stokes equation as the Knudsen number tends to zero. Here we relate M, K to viscosity and heat conduction coefficients by defining functions $\mu(\text{Kn}) = \frac{3\mu_0}{4}M(\text{Kn})$ and $\kappa(\text{Kn}) = \kappa_0 K(\text{Kn})$, where μ_0, κ_0 are viscosity and heat conduction coefficients of the gas respectively. Under this setting we impose the natural constraints

$$\begin{aligned}\mu_0 &= \lim_{\text{Kn} \rightarrow 0} \mu(\text{Kn}), \\ \kappa_0 &= \lim_{\text{Kn} \rightarrow 0} \kappa(\text{Kn}).\end{aligned}\quad (6)$$

In addition we use the following relation

$$\kappa(\text{Kn}) = \frac{5k_B}{2m} \frac{\mu(\text{Kn})}{\text{Pr}}, \quad \text{Pr} = \frac{2}{3} \quad (7)$$

to constraint the Prandtl number Pr to the Chapman-Enskog result $\text{Pr} = \frac{2}{3}$, so in essence we couple κ and μ together. While for training our model this coupling isn't necessary, we have chosen to do so because it makes sense physically, and it does accelerate the learning process without undermining the accuracy. Finally the derivatives of $\mu(\text{Kn}), \kappa(\text{Kn})$ will tend to zero as the Knudsen number tends to zero. To satisfy all these constraints, we design the following modified fully connected neural network

$$\begin{aligned}M(\text{Kn}) &= \frac{4}{3}(1 + \mathcal{N}(\text{Kn})) \\ \mathcal{N}(\text{Kn}) &= \mathbf{W}_2 \cdot \text{Tanh}(\mathbf{W}_1 \cdot \mathcal{H}(20\text{Kn})) \\ \mathcal{H}(x) &= \frac{1}{2}x^2, \quad x < 1 \\ &= |x| - \frac{1}{2}, \quad x \geq 1,\end{aligned}\quad (8)$$

in which $\mathbf{W}_1, \mathbf{W}_2$ are the one-dimension weights vector of the neural network, with the activation function Tanh acting element-wise on the vector input. The function $\mathcal{N}(\text{Kn})$ satisfies $\mathcal{N}(0) = \mathcal{N}'(0) = 0$. Therefore we guaranteed consistency with the NS equation.

The next step will be learning the weights vector $\mathbf{W}_1, \mathbf{W}_2$ in the neural network from data. This requires a loss function as the learning target. In our case, the loss function compares the difference between the observed spectra $\langle \rho^2 \rangle_{dsmc}$ and predicted spectra $\langle \rho^2 \rangle$. The former are results from the DSMC method, while the latter

are the predictions of the governing equation (3) and the constitutive relations (5) and (7). We define the loss function for any input weight vector $\mathbf{W} = \mathbf{W}_1, \mathbf{W}_2$ as

$$L(\mathbf{W}) = \mathbb{E}_{\text{Kn} \sim U} \mathbb{E}_{\omega \sim p(\omega|\text{Kn})} \left| \langle \rho^2 \rangle_{dsmc}(\text{Kn}, \omega) - \langle \rho^2 \rangle(\text{Kn}, \omega; \mathbf{W}) \right|^2, \quad (9)$$

in which spectra are functions on ω and the Knudsen number, and the predicted spectra $\langle \rho^2 \rangle$ is a function on the weights vectors \mathbf{W} because it depends on the neural network $M(\text{Kn})$. The symbol $\mathbb{E}_{\text{Kn} \sim U}$ represents taking the expectation numerically by sampling Kn from a uniform distribution U . Meanwhile, $\mathbb{E}_{\omega \sim p(\omega|\text{Kn})}$ represents taking the expectation by sampling ω from a conditional distribution $p(\omega|k)$, which is proportional to the amplitude of the DSMC spectra. Sampling ω in this way makes the sample point lies more in the peak region. After defining the loss function, we use the ADAM [25] optimizer to minimize the loss function. The unknown coefficients \mathbf{W} are therefore determined.

Until now, we have introduced the DUAL model, which could be divided into two processes: inference and training. The inference process calculates the density fluctuation spectra using the governing equations (3) and the constitutive relations (5). The constitutive relations contain neural networks M, K defined in (8) and (7) with weights to be determined. The training process determines the weights of neural networks by minimizing the loss function (9). The flow chart Fig 2 summarizes the entire procedure.

Results We compare the density fluctuation spectra calculated by the DUAL model with the results of the NS equation and the Grad 13 method. For various Knudsen numbers, spectra $\langle \delta \tilde{\rho}^2 \rangle(\tilde{\omega})$ are shown in Fig 3 as function of the non-dimensionalized frequency $\tilde{\omega}$. At a small Knudsen number, all models give consistent spectra. However, At large Knudsen number, the DUAL model result matches nicely with the DSMC result, while the shape and amplitude of the NS equation and Grad 13 moments method deviate. Therefore, compared with the NS equation and the Grad 13 method, our DUAL model gives the most accurate spectra which are close to the DSMC result in both shape and amplitude.

We test the DUAL model performance on predicting the velocity fluctuation spectra to show its generalization ability. The generalization ability ensures that, rather than force to reproduce the DSMC spectra, the DUAL model learns the rarefied dynamic physics. To prove it did learn physics, we let the DUAL model predicts the velocity fluctuation spectra which the DUAL model has never seen as data. The result is shown in Fig 4(a). The DUAL model gives the correct shape that is much better than the NS equation. Consequently, our DUAL model has the generalization ability to predict spectra of other quantities, hence did learn the rarefied dynamic physics.

The rarefied dynamic physics learned from data is encoded in neural network M . We plot the neural network M in Fig 4(b) as the function $M(\text{Kn})$ multiplied by Kn .

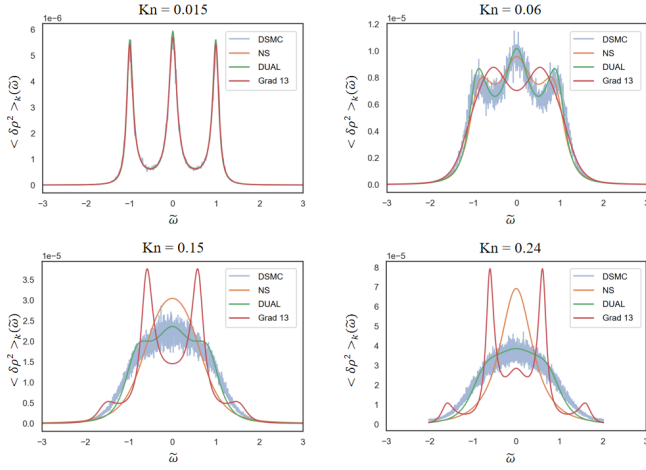


FIG. 3. Comparison between spectra calculated using DSMC, the NS equation, the Grad 13 method, and the DUAL model for various Knudsen numbers. At a small Knudsen number, The spectra consist of three peaks: The central one due to the entropy fluctuation which corresponds to the heat diffusion, and two peaks on each side due to pressure fluctuation corresponding to sound wave propagation. As the Knudsen number increase, the peaks of the spectra disappear gradually and blur into a bell shape. The result showed that the DUAL model calculated spectra match the DSMC result much better than the NS equation and Grad 13 method, especially in the high Knudsen number region.

The corresponding function for the NS equation is also plotted because the NS equation also lies in the DUAL model framework. At the origin, these two plots are tangent, indicating the DUAL model is consistent with the NS equation. As the Knudsen number increase, the plot for the DUAL model bends downward. This downward bend means that viscosity decrease as the Knudsen number increase, as we will discuss later.

Discussion The DUAL model showed that the data-driven approach has the advantage over perturbation and moment expansion methods, corresponding to the NS equation and the Grad 13 method accordingly. Limited by their slow convergence rate at large Knudsen number, higher-order perturbation or moment expansion benefit little for more accurate spectra at large Knudsen numbers[26]. Instead, the DUAL model learns the rarefied gas dynamics from data points equally, hence converge uniformly for various Knudsen numbers. As we have shown in the result section, the DUAL model outperforms the NS equation and the Grad 13 method using only three conservation laws. Therefore the data-driven approach has demonstrated a clear advantage in handling rarefied gas dynamics.

Another reason that the DUAL model can learn rarefied gas dynamics is that it has a clear physical meaning: The DUAL model is equivalent to a Knudsen number adaptive viscosity. This equivalence could be deduced from (6), in which the viscosity coefficient μ_0 is the limit-

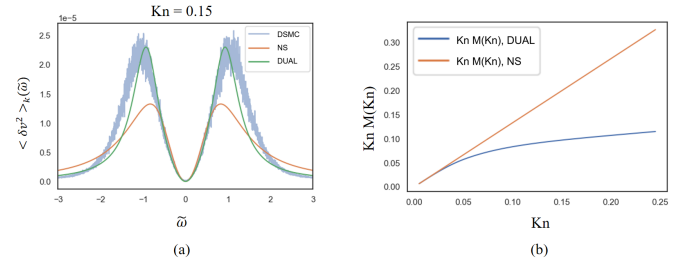


FIG. 4. (a) The test comparison between the DUAL model and NS equation predicted velocity fluctuation spectra with DSMC results at Knudsen number $Kn = 0.15$. Though the DUAL model has never trained on the velocity fluctuation spectra, it still outperforms the NS equation. Therefore the DUAL model has generalization ability, hence did learn the rarefied dynamic physics. (b) The function $M(Kn)$ multiplied with Kn inferred from DSMC data by the DUAL model, compared with the corresponding function for the NS equation. They are consistent when the Knudsen number is small.

ing case of the non-negative term $\frac{3\mu_0}{4}M(Kn)$. We define this term as a viscosity coefficient $\mu(Kn)$ that depends on the Knudsen number. Since viscosity increases entropy as long as the viscosity coefficient is positive, the entropy of the system is non-decreasing. Therefore the DUAL model satisfies the second law of thermodynamics by equivalence with viscosity.

Equivalence with viscosity does not limit the flexibility of the DUAL model. Instead, the DUAL model is sufficient to model all well-defined linear constitutive relations. The well-defined constitution relations refer to that consist of spatial derivatives and satisfy the second law of thermodynamics. The reason is as follows. Firstly, we claim that the constitution relation for stress consists of velocity derivatives, while the constitution relation for heat flux consists of temperature derivatives

$$\begin{aligned}\sigma &= -\sum_{n=1}^{\infty} a_n \frac{\partial^n v_x}{\partial x^n} \\ q &= -\sum_{n=1}^{\infty} b_n \frac{\partial^n T}{\partial x^n},\end{aligned}\quad (10)$$

where a_n, b_n are coefficients. This is because velocity fluctuates independently with temperature[27], but the stress and velocity, same as heat flux and temperature, must be correlated to produce non-increasing entropy

$$\dot{s} = -\frac{q_j}{T^2} \partial_j T - \frac{\sigma_{ij}}{2T} \left(\frac{\partial v_i}{\partial x_j} + \frac{\partial v_j}{\partial x_i} \right), \quad (11)$$

where \dot{s} is the entropy change rate per mass. The only possibility is stress depends on velocity only, the same as heat flux depending on temperature. Secondly, even-order derivatives vanish in constitution relation (10) because the entropy change rate (11) must be real and non-negative in the Fourier space. Finally, sum over the infinite series (10) in the Fourier space can be shown to be

equivalent to the DUAL model constitution relation (5). Therefore the DUAL model is flexible enough.

Of course, the DUAL model still has its limitations. It is expected to be unsuitable for strong non-equilibrium dynamics, such as shock waves. Counter-intuitively, the reason for the unsuitability is a lack of constraints rather than flexibility. The flexibility on constitutive relation to model stress and heat flux freely comes with a price: We are limited to near-equilibrium dynamics. More explicitly, near-equilibrium dynamics refer to the one-particle distribution $f(\mathbf{c})$ for gas molecule velocity in the non-dimensionalized form

$$\begin{aligned} f &= f_0(1 + h) \\ h &= \frac{3}{4}\text{Kn}(c_i c_j - \frac{1}{3}\delta_{ij}\mathbf{c}^2)\sigma_{ij} + \frac{\text{Kn}}{\text{Pr}}(\frac{\mathbf{c}^2}{2} - \frac{5}{2})c_i q_i, \end{aligned} \quad (12)$$

where \mathbf{c} is the non-dimensional peculiar velocity, and f_0 is the Maxwell distribution. It is the only form of f that admits arbitrary stress σ and heat flux q as its moments. Consequently it has no further expressibility for strong non-equilibrium dynamics, such as when irregular shape f appears in shock wave dynamics. To model such dynamics, more expressibility for f is necessary. As a trade-off, we must impose proper constraints on constitutive

relations. This observation indicates that investigating proper constraints is the direction for a constitutive relation for strong non-equilibrium dynamics.

In summary, we have proposed a robust, Knudsen-number-dependent constitutive relation model for rarefied gas dynamics. As a crucial step towards general and practical data-driven modeling, we have extended the data-driven approach from Knudsen-number-specific to Knudsen-number-dependent. This gives the model the ability to adapt to the Knudsen number change in practice. In addition, we have shown that by designing the model carefully, consistency with limiting cases and agreement with constraints such as non-decreasing entropy could be achieved. However, future development is still needed for our model to accommodate more complex benchmarks such as non-homogeneous cases and more complex dynamics such as strong non-equilibrium dynamics.

ACKNOWLEDGMENTS

We wish to acknowledge the support of Professor Lei Wu at Southern University of Science and Technology in offering suggestions.

-
- [1] E. P. Muntz, Rarefied Gas Dynamics, Annual Review of Fluid Mechanics 10.1146/annurev.fl.21.010189.002131 (1989).
- [2] Spacecraft charging: A review, in *Space Systems and Their Interactions with Earth's Space Environment*, pp. 167–226.
- [3] G. Fiocco and J. DeWolf, Frequency spectrum of laser echoes from atmospheric constituents and determination of the aerosol content of air, Journal of Atmospheric Sciences **25**, 488 (1968).
- [4] L. Boltzmann, *Lectures on gas theory* (Courier Corporation, 2012).
- [5] C. W. Kilmister and C. Cercignani, The Boltzmann Equation and Its Applications, The Mathematical Gazette 10.2307/3618229 (1989).
- [6] G. A. Bird, Molecular gas dynamics and the direct simulation of gas flows - 2nd edition (1994).
- [7] D. Hilbert, Begründung der kinetischen Gastheorie, Mathematische Annalen 10.1007/BF01456676 (1912).
- [8] VI. On the law of distribution of molecular velocities, and on the theory of viscosity and thermal conduction, in a non-uniform simple monatomic gas, Philosophical Transactions of the Royal Society of London. Series A, Containing Papers of a Mathematical or Physical Character 10.1098/rsta.1916.0006 (1916).
- [9] D. Enskog, Kinetische theorie der vorgänge in mässig verdünnten gasen. i. allgemeiner teil, Uppsala: Almqvist & Wiksells Boktryckeri (1917).
- [10] H. Grad, On the kinetic theory of rarefied gases, Communications on Pure and Applied Mathematics **2**, 331 (1949).
- [11] M. Raissi, P. Perdikaris, and G. E. Karniadakis, Machine learning of linear differential equations using Gaussian processes, Journal of Computational Physics 10.1016/j.jcp.2017.07.050 (2017), arXiv:1701.02440.
- [12] S. H. Rudy, S. L. Brunton, J. L. Proctor, and J. N. Kutz, Data-driven discovery of partial differential equations, Science Advances 10.1126/sciadv.1602614 (2017), arXiv:1609.06401.
- [13] H. Schaeffer, Learning partial differential equations via data discovery and sparse optimization, Proceedings of the Royal Society A: Mathematical, Physical and Engineering Sciences 10.1098/rspa.2016.0446 (2017).
- [14] M. Raissi, P. Perdikaris, and G. E. Karniadakis, Physics-informed neural networks: A deep learning framework for solving forward and inverse problems involving nonlinear partial differential equations, Journal of Computational Physics 10.1016/j.jcp.2018.10.045 (2019).
- [15] Z. Long, Y. Lu, X. Ma, and B. Dong, PDE-Net: Learning PDEs from data, in *6th International Conference on Learning Representations, ICLR 2018 - Workshop Track Proceedings* (2018).
- [16] Z. Long, Y. Lu, and B. Dong, PDE-Net 2.0: Learning PDEs from data with a numeric-symbolic hybrid deep network, Journal of Computational Physics **399**, 10.1016/j.jcp.2019.108925 (2019), arXiv:1812.04426.
- [17] Y. LeCun, Y. Bengio, *et al.*, Convolutional networks for images, speech, and time series, The handbook of brain theory and neural networks **3361**, 1995 (1995).
- [18] N. Dal Santo, S. Deparis, and L. Pegolotti, Data driven approximation of parametrized PDEs by reduced basis and neural networks, Journal of Computational Physics **416**, 109550 (2020), arXiv:1904.01514.
- [19] J. Zhang and W. Ma, Data-driven discovery of governing

equations for fluid dynamics based on molecular simulation, *Journal of Fluid Mechanics* 10.1017/jfm.2020.184 (2020).

- [20] J. Hana, C. Ma, Z. Ma, and E. Weinan, Uniformly accurate machine learning-based hydrodynamic models for kinetic equations, *Proceedings of the National Academy of Sciences of the United States of America* 10.1073/pnas.1909854116 (2019).
- [21] S. Yip and M. Nelkin, Application of a kinetic model to time-dependent density correlations in fluids, *Physical Review* **135**, 10.1103/PhysRev.135.A1241 (1964).
- [22] J. D. Jackson, *Classical electrodynamics* (1999).
- [23] L. D. Landau, *The classical theory of fields*, Vol. 2 (Elsevier, 2013).
- [24] R. Pecora, Doppler shifts in light scattering from pure liquids and polymer solutions, *The Journal of Chemical Physics* **40**, 1604 (1964).
- [25] D. P. Kingma and J. L. Ba, Adam: A method for stochastic optimization, in *3rd International Conference on Learning Representations, ICLR 2015 - Conference Track Proceedings* (2015) arXiv:1412.6980.
- [26] L. Wu and X.-J. Gu, On the accuracy of macroscopic equations for linearized rarefied gas flows, *Advances in Aerodynamics* **2**, 10.1186/s42774-019-0025-4 (2020).
- [27] L. D. Landau and E. M. Lifshitz, *Statistical Physics part II* (1980).
- [28] J. C. Maxwell, Iv. on the dynamical theory of gases, *Philosophical transactions of the Royal Society of London*, 49 (1867).
- [29] J. Friedman, T. Hastie, R. Tibshirani, *et al.*, *The elements of statistical learning*, Vol. 1 (Springer series in statistics New York, 2001).
- [30] R. Tibshirani, Regression shrinkage and selection via the lasso, *Journal of the Royal Statistical Society: Series B (Methodological)* **58**, 267 (1996).
- [31] S. Chapman and T. G. Cowling, *The mathematical theory of non-uniform gases: an account of the kinetic theory of viscosity, thermal conduction and diffusion in gases* (Cambridge university press, 1990).
- [32] D. Burnett, The distribution of molecular velocities and the mean motion in a non-uniform gas, *Proceedings of the London Mathematical Society* **s2-40**, 382 (1936).
- [33] L. D. Landau and E. M. Lifshitz, *Fluid mechanics: Landau and Lifshitz: course of theoretical physics* (1987), arXiv:1003.3921v1.

Appendix A: Rayleigh Scattering Background

The Rayleigh scattering has been discovered by Lord Rayleigh back in the nineteenth century. It is the reason for the blue color of the sky in daytime and twilight. As we have mentioned in the method section, the Rayleigh scattering describes the refraction of electromagnetic waves (EM waves) passing through media with density fluctuation, which leads to refraction index fluctuation[22, 23]. Considering incident wave as plain EM wave with given wavevector \mathbf{k}_i ,

$$\begin{aligned} \mathbf{E}_{inc} &= \boldsymbol{\xi}_0 \exp(i\mathbf{k}_i \cdot \mathbf{r} - i\omega_i t) \\ |\mathbf{k}_i| &= \frac{\sqrt{\epsilon_0}\omega_i}{c} \end{aligned} \quad (\text{A1})$$

With $\boldsymbol{\xi}_0$ be the polarization vector, \mathbf{k}_i the incident wave vector, ω_i the incident wave frequency, and ϵ_0 the dielectric constant of gas. The refraction index fluctuation is proportional to the dielectric constant of the gas $\epsilon(\rho)$, hence related to the density fluctuation to the density fluctuation as the following perturbation relation

$$\epsilon = \epsilon_0 + \partial_\rho \epsilon(\rho_0) \delta\rho + \dots \quad (\text{A2})$$

where the ρ_0 is the density of gas and $\delta\rho$ is the fluctuation of the gas density. The scattered spectra I is defined by the autocorrelation function of scattered electric field \mathbf{E}_1 .

$$\mathbf{I}(\omega_f) = \frac{1}{2\pi} \int \langle \mathbf{E}_1(t') \cdot \mathbf{E}_1(t' + t) \rangle \exp(-i\omega_f t) dt \quad (\text{A3})$$

In which the $\langle Q \rangle$ means the ensemble average of the quantity Q . The scattered spectra I could be calculated by perturbation method is as follows according to [24]

$$\begin{aligned} \mathbf{I}(\omega_f) &= \frac{N\omega_i^4 |\boldsymbol{\xi}_0|^2 \sin^2(\psi)}{32\pi^3 c^4 r^2} [\partial_\rho \epsilon(\rho_0)]^2 \\ &\int dt \int d\mathbf{r}^3 e^{-i(\omega_f - \omega_i)t} e^{-i(\mathbf{k}_i - \mathbf{k}_f) \cdot \mathbf{r}} (G(\mathbf{r}, t) - \rho_0) \\ G(\mathbf{r}, t) &= \frac{1}{N} \left\langle \int d\mathbf{r}'^3 \rho(\mathbf{r}' - \mathbf{r}, 0) \rho(\mathbf{r}', t) \right\rangle \end{aligned} \quad (\text{A4})$$

in which the G is the so-called density correlation function. N represents the total number of gas molecules we are considering in our integration domain, \mathbf{k}_f the scattered wave vector, ω_f the scattered wave frequency, c is the speed of light in vacuum and r is the distance between the scattering gas medium and observer. It is easy to derive that the term inside the integral of first equation in A4 is proportional to the density fluctuation spectra $\langle \rho^2 \rangle(\mathbf{k}_i - \mathbf{k}_f, \omega_i - \omega_f)$ for given $\mathbf{k}_i, \mathbf{k}_f$. The density fluctuation spectra is defined as, for density function $\rho(t)$, that

$$\begin{aligned} \langle \rho^2 \rangle(\omega, \mathbf{k}) &= \frac{1}{2\pi} \int \langle \rho^2 \rangle(t, \mathbf{x}) e^{-i\omega t} e^{-i\mathbf{k} \cdot \mathbf{x}} dt d\mathbf{x} \\ \langle \rho^2 \rangle(t, \mathbf{x}) &= \langle \rho(t_0, \mathbf{x}_0) \rho(t_0 + t, \mathbf{x}_0 + \mathbf{x}) \rangle \end{aligned} \quad (\text{A5})$$

In summary, the key of calculating the Rayleigh scattering spectra is to calculate the density fluctuation spectra.

Appendix B: Non-dimensionalization of the governing equation

In system equation (3), the non-dimensionalization use the reference length scale $\Delta x = \frac{2\pi}{k}$, and the reference time scale follows $\frac{\Delta x}{\Delta t} = \sqrt{\frac{k_B T_0}{m}}$. The non-dimensionalized quantity is represented with bar as $\bar{t} = \frac{t}{\Delta t}$, $\bar{x} = \frac{x}{\Delta x}$, $\bar{v}_x = \frac{\Delta t v_x}{\Delta x}$, $\bar{\rho} = \frac{\rho - \rho_0}{\rho_0}$, $\bar{T} = \frac{T - T_0}{T_0}$, $\bar{\sigma}_{xx} = \frac{m}{\rho_0 k_B T_0} \sigma_{xx}$, $\bar{q}_x = \frac{1}{\rho_0} \left(\frac{m}{k_B T_0} \right)^{3/2} q_x$.

Appendix C: Derivation of the DUAL model from linear combination of derivatives

This section we will show that the DUAL model (5) is flexible enough to model all well defined linear constitutive relations. As we discussed in the paper, the well defined linear constitutive relations are of the form (10) under the condition of non-increasing entropy. We will show that the DUAL model could be derived from these linear constitutive relations. The non-dimensionalized form of these well defined linear constitutive relations are

$$\begin{aligned}\bar{\sigma}_{xx} &= -\sum_{n=1}^{\infty} \frac{a_n}{\mu\Delta x^{n-1}} \frac{\partial^n \bar{v}_x}{\partial \bar{x}^n} = -\sum_{n=1}^{\infty} \bar{a}_n \frac{\partial^n \bar{v}_x}{\partial \bar{x}^n} \\ \bar{q}_x &= -\sum_{n=1}^q \frac{b_n}{\kappa\Delta x^{n-1}} \frac{\partial^n \bar{T}}{\partial \bar{x}^n} = -\sum_{n=1}^q \bar{b}_n \frac{\partial^n \bar{T}}{\partial \bar{x}^n}\end{aligned}\quad (\text{C1})$$

in which $\bar{a}_n = \frac{a_n}{\mu\Delta x^{n-1}}$, $\bar{b}_n = \frac{b_n}{\kappa\Delta x^{n-1}}$. These non-dimensional quantities having no constraints on them yet. An analysis on entropy change of the system, using equation 11, tells us that

$$q_j \partial_j T \leq 0; \quad \sigma_{ij} \left(\frac{\partial v_i}{\partial x_j} + \frac{\partial v_j}{\partial x_i} \right) \leq 0. \quad (\text{C2})$$

We require the two term independently satisfy these condition because the temperature and velocity fluctuation independently. In our 1D case, more explicitly, we have

$$q_x \partial_x T \leq 0; \quad \sigma_{xx} \partial_x v_x \leq 0 \quad (\text{C3})$$

Especially, in our case, the system is homogeneous, hence there should not exist a particular scale that entropy decrease. We expect no entropy production for each scale. Hence if we decompose the system in Fourier modes, we wish to have

$$\tilde{q}_k (ik\tilde{T}_k)^* \leq 0; \quad \tilde{\sigma}_k (ik\tilde{v}_k)^* \leq 0 \quad (\text{C4})$$

The * indicates complex conjugate. Combine with our linear model 10, after a Fourier transformation on spatial coordinate, we have the condition

$$\begin{aligned}\sum_{n=1}^{\infty} (ik)^{n+1} a_n |\tilde{v}_k|^2 &\leq 0 \\ \sum_{n=1}^{\infty} (ik)^{n+1} b_n |\tilde{T}_k|^2 &\leq 0\end{aligned}\quad (\text{C5})$$

The previous equation, requires that there are no imaginary part on the LHS. Hence only terms with even powers on i remains, as follows

$$\begin{aligned}(k^2 a_1 - k^4 a_3 + k^6 a_5 - k^8 a_7 \dots) |\tilde{v}_k|^2 &\geq 0 \\ (k^2 b_1 - k^4 b_3 + k^6 b_5 - k^8 b_7 \dots) |\tilde{T}_k|^2 &\geq 0\end{aligned}\quad (\text{C6})$$

In our case, the Knudsen number is determined directly by the wave number k , as shown in 2. In addition, we want the only non-dimensional quantity that govern the system to be the Knudsen number Kn . Hence we expect quantities \bar{a}, \bar{b} to be functions of the Knudsen number. The non-dimensionalized version of the constitutive relation is as

$$\begin{aligned}\partial_{\bar{x}} \bar{\sigma}(\bar{k}) &= (\bar{k}^2 \bar{a}_1 - \bar{k}^4 \bar{a}_3 + \bar{k}^6 \bar{a}_5 \dots) \tilde{v}_{\bar{k}} = \bar{k}^2 M(\bar{k}) \tilde{v}_{\bar{k}} \\ \partial_{\bar{x}} \bar{q}(\bar{k}) &= (\bar{k}^2 \bar{b}_1 - \bar{k}^4 \bar{b}_3 + \bar{k}^6 \bar{b}_5 \dots) \tilde{T}_{\bar{k}} = \bar{k}^2 K(\bar{k}) \tilde{T}_{\bar{k}},\end{aligned}\quad (\text{C7})$$

in which function M, K are the infinite sum of series and should be nonnegative functions. Besides, $\bar{k} = \frac{k\Delta x}{2\pi}$ is the non-dimensionalized version of k . Particularly, the non-dimensionalized \bar{k} is proportional to the Knudsen number by (2). We could further deduce the stress and heat flux as the DUAL model:

$$\begin{aligned}\bar{\sigma}(\bar{k}) &= -i\bar{k}M(Kn)\tilde{v}_{\bar{k}} \quad M(Kn) \geq 0 \\ \bar{q}(\bar{k}) &= -i\bar{k}K(Kn)\tilde{T}_{\bar{k}} \quad K(Kn) \geq 0.\end{aligned}\quad (\text{C8})$$

Appendix D: Calculating the density fluctuation spectra

Substitute the DUAL model into (3), for monatomic gas with the heat conduction coefficient $\kappa = \frac{15k_B}{4m}\mu$, we have the non-dimensionalized system equation to be

$$\begin{aligned}\partial_{\bar{t}} \delta \bar{\rho} + \partial_{\bar{x}} \bar{v}_x &= 0 \\ \partial_{\bar{t}} \bar{v}_x + \partial_{\bar{x}} \delta \bar{T} + \partial_{\bar{x}} \delta \bar{\rho} &= Kn \sum_{n=1}^{\infty} \bar{a}_n \partial_{\bar{x}}^{n+1} \bar{v}_x \\ \frac{3}{2} \partial_{\bar{t}} \delta \bar{T} + \partial_{\bar{x}} \bar{v}_x &= \frac{15}{4} Kn \sum_{n=1}^{\infty} \bar{b}_n \partial_{\bar{x}}^{n+1} \bar{T}\end{aligned}\quad (\text{D1})$$

Multiply $\rho(0,0)$ and take ensemble average, we could obtain a system on correlation functions such as $\langle \rho^2 \rangle(t, x)$, $\langle \rho v_x \rangle(t, x)$, etc. These functions are well defined since we are considering homogeneous gas, hence the fluctuations are stationary.

Before we proceed, we define the one-sided Fourier transform on time coordinate:

$$x_{\omega}^{(+)} = \frac{1}{\sqrt{2\pi}} \int_0^{\infty} x(t) e^{-i\omega t} dt. \quad (\text{D2})$$

And in this section we omit the bar that indicates non-dimensionalized variables.

Doing a Fourier transform on space coordinate, and one-sided Fourier transformation on time coordinate, the

macroscopic equation becomes

$$\begin{aligned}
i\omega \langle \rho^2 \rangle_{\omega,k}^+ + ik \langle \rho v_x \rangle_{\omega,k}^+ &= \frac{1}{\sqrt{2\pi}} \langle \rho^2 \rangle_k \\
i\omega \langle \rho v_x \rangle_{\omega,k}^+ + ik \langle \rho T \rangle_{\omega,k}^+ + ik \langle \rho^2 \rangle_{\omega,k}^+ &= \\
&\quad -k^2 \text{Kn} M(\text{Kn}) \langle \rho v_x \rangle_{\omega,k}^+ \\
\frac{3}{2} i\omega \langle \rho T \rangle_{\omega,k}^+ + ik \langle \rho v_x \rangle_{\omega,k}^+ &= -\frac{15}{4} k^2 \text{Kn} K(\text{Kn}) \langle \rho T \rangle_{\omega,k}^+
\end{aligned} \tag{D3}$$

The term $\langle \rho^2 \rangle_k$ on the left hand side of the first equation in D3 comes from integration by part. This is the spatial density fluctuation spectra which is a constant, since there are no spatial correlation between different location at macroscopic level. The term $\langle \tilde{\rho}^2 \rangle_k$ could be calculated from fluctuation theory [27, 33]

$$\langle \rho^2 \rangle_k = \frac{m N_{eff} k}{(2\pi)^{3/2} \rho_0} \tag{D4}$$

Where the m is the molecule mass, and the N_{eff} is the

effective number of molecules per particle used in the DSMC simulation, to take the Monte Carlo fluctuation into account. The integration by part will also give terms such as $\langle \rho v \rangle_k$ and $\langle \rho T \rangle_k$. However, it is known that they vanish according to fluctuation theory.

The density fluctuation spectra could be obtained from the spectra $\langle \tilde{\rho}^2 \rangle_{\omega,k}^+$ which takes one sided Fourier transform on time coordinate and Fourier transform on spatial coordinate. The following relation could be used to obtain the density fluctuation spectra:

$$\langle \rho^2 \rangle_{\omega} = \langle \rho^2 \rangle_{\omega}^{(+)} + \langle \rho^2 \rangle_{\omega}^{(+)*} \tag{D5}$$

Substitute the linear constitutive relation model into the system equation, we have the system D3, combined with the initial condition D4. The term $\langle \rho^2 \rangle_{\omega,k}^+$ could be solved from the system, with the notation

$$\begin{aligned}
A(\text{Kn}) &= \text{Kn} M(\text{Kn}) \\
B(\text{Kn}) &= \frac{15}{4} \text{Kn} K(\text{Kn}).
\end{aligned} \tag{D6}$$

The solution for $\langle \rho^2 \rangle_{\omega,k}^+$ is

$$\langle \rho^2 \rangle_{\omega,k}^+ = -\frac{ik N_{eff} m (-2k^4 A(\text{Kn}) B(\text{Kn}) - 3ik^2 \omega A(\text{Kn}) - 2ik^2 \omega B(\text{Kn}) - 2k^2 + 3\omega^2)}{(2\pi)^2 \rho_0 (-2k^4 \omega A(\text{Kn}) B(\text{Kn}) - 3ik^2 \omega^2 A(\text{Kn}) + 2ik^4 B(\text{Kn}) - 2ik^2 \omega^2 B(\text{Kn}) - 5k^2 \omega + 3\omega^3)} \tag{D7}$$

The NS equation also lies in the framework of linear constitutive relation model. We just need to set the following relation

$$M(\text{Kn}) = \frac{4}{3} \tag{D8}$$

combine with equation 7. The spectra hence follows the same form as in equation D7.

As for the Grad 13 method, two addition equation on

the stress and heat flux appears. as is

$$\begin{aligned}
\partial_t \sigma + \frac{4}{3} \partial_x v_x + \frac{8}{15} \partial_x q &= -\frac{\sigma}{\text{Kn}} \\
\partial_t q + \partial_x \sigma + \frac{5}{2} \partial_x T &= -\frac{2}{3} \frac{q}{\text{Kn}}
\end{aligned} \tag{D9}$$

Again, Multiply $\rho(0,0)$ and take ensemble average, we could obtain another system on correlation functions. Doing a one sided Fourier transformation on time and Fourier transformation on space coordinates, we have

$$\begin{aligned}
i\omega \langle \rho^2 \rangle_{\omega,k}^+ + ik \langle \rho v_x \rangle_{\omega,k}^+ &= \frac{m N_{eff} k}{(2\pi)^2 \rho_0} \\
i\omega \langle \rho v_x \rangle_{\omega,k}^+ + ik \langle \rho T \rangle_{\omega,k}^+ + ik \langle \rho^2 \rangle_{\omega,k}^+ + ik \langle \rho \sigma \rangle_{\omega,k}^+ &= 0 \\
\frac{3}{2} i\omega \langle \rho T \rangle_{\omega,k}^+ + ik \langle \rho v_x \rangle_{\omega,k}^+ + ik \langle \rho q \rangle_{\omega,k}^+ &= 0 \\
i\omega \langle \rho \sigma \rangle_{\omega,k}^+ + \frac{4}{3} ik \langle \rho v_x \rangle_{\omega,k}^+ + \frac{8}{15} ik \langle \rho q \rangle_{\omega,k}^+ &= -\frac{\langle \rho \sigma \rangle_{\omega,k}^+}{\text{Kn}} \\
i\omega \langle \rho q \rangle_{\omega,k}^+ + ik \langle \rho \sigma \rangle_{\omega,k}^+ + \frac{5}{2} ik \langle \rho T \rangle_{\omega,k}^+ &= -\frac{2 \langle \rho q \rangle_{\omega,k}^+}{3 \text{Kn}}
\end{aligned} \tag{D10}$$

The spectra is hence calculated in the same way as NS

equation and linear constitutive relation model. The

result is

$$\langle \delta \rho^2 \rangle_{\omega, k, Grad13}^+ = \frac{m N_{\text{eff}} k (-36 i k^4 \text{Kn}^2 + 189 i k^2 \text{Kn}^2 \omega^2 + 165 k^2 \text{Kn} \omega - 20 i k^2 - 45 i \text{Kn}^2 \omega^4 - 75 \text{Kn} \omega^3 + 30 i \omega^2)}{(2\pi)^2 \rho_0 (135 k^4 \text{Kn}^2 \omega - 75 i k^4 \text{Kn} - 234 k^2 \text{Kn}^2 \omega^3 + 240 i k^2 \text{Kn} \omega^2 + 50 k^2 \omega + 45 \text{Kn}^2 \omega^5 - 75 i \text{Kn} \omega^4 - 30 \omega^3)} \quad (\text{D11})$$

As for the velocity fluctuation spectra, the LHS of D3 need to be modified, since this time we product $v_x(0, 0)$

instead of $\rho(0, 0)$ before taking the ensemble average. This time we have

$$\begin{aligned} i\omega \langle \rho v_x \rangle_{\omega, k}^+ + ik \langle v_x^2 \rangle_{\omega, k}^+ &= 0 \\ i\omega \langle v_x^2 \rangle_{\omega, k}^+ + ik \langle v_x T \rangle_{\omega, k}^+ + ik \langle \rho v_x \rangle_{\omega, k}^+ &= -k^2 A(\text{Kn}) \langle \rho v_x \rangle_{\omega, k}^+ + \frac{N_{\text{eff}} m k}{(2\pi)^2 \rho_0} \\ \frac{3}{2} i\omega \langle v_x T \rangle_{\omega, k}^+ + ik \langle v_x^2 \rangle_{\omega, k}^+ &= -k^2 B(\text{Kn}) \langle v_x T \rangle_{\omega, k}^+ \end{aligned} \quad (\text{D12})$$

$$\langle \delta v_x^2 \rangle_{\omega, k}^+ = -\frac{i N_{\text{eff}} m \omega k (3\omega - 2ik^2 B(\text{Kn}))}{(2\pi)^2 \rho (-2k^4 \omega A(\text{Kn}) B(\text{Kn}) - 3ik^2 \omega^2 A(\text{Kn}) + 2ik^4 B(\text{Kn}) - 2ik^2 \omega^2 B(\text{Kn}) - 5k^2 \omega + 3\omega^3)} \quad (\text{D13})$$

Appendix E: DSMC calculation Details

We use the DSMC0F program by A.Bird [6] to simulate the fluctuation of 1D homogeneous gas. The computing details are shown in following Table I using SI units. A snap shot will be stored for every 5 time steps. Then the macroscopic quantities for each cell are calculated by averaging corresponding quantites of particles in each cell. The density fluctuation spectra used to train the neural network is ensemble average from 27 independent DSMC run.

Appendix F: Neural Network Training Details

The density fluctuation spectra is of the form $\langle \rho^2 \rangle(k, \omega)$, with k corresponds to the wave number of our interested density fluctuation wave, which directly determines the Knudsen number, and ω be the frequency of the corresponding wave. Given k , the spectra $\langle \rho^2 \rangle_k(\omega)$ is a function of the angular frequency ω with spectra structure caused by collective behavior of gas molecules. Duirng training process of linear constitutive relation model, 200 k is draw from a uniform distribution on the interval $\left[0, \frac{\pi \rho_0}{2\mu} \sqrt{\frac{k_B T_0}{m}}\right]$. for a given k , we do a Monte Carlo sample using acceptance-rejection method, 200 draw of ω from the range $[-3ck, 3ck]$ with probabil-

TABLE I. The coefficients and configuration used in DSMC0F program.

Domain Length	4.8	Collision Model	VHS ^a
Power law ^b	0.5	Diameter ^c	3.5×10^{-10}
Num of Cell	1281	Mean Free Path	1.8×10^{-2}
Simulation Particle	128100	Mean Free Time	4×10^{-5}
Density	5×10^{-6}	Temperature	300
Molecule Mass	5×10^{-26}	Sound Speed	371.56
Heat Conduction	0.0214	Viscosity	2.07×10^{-5}
Δt	4×10^{-6}	Δx	3.7×10^{-3}
Subcell ^d	8		

^a Variable hard sphere model

^b The viscosity-temperature power law used in variable hard sphere model

^c The reference molecule diameter

^d The number of subcell per cell used in particle collision process

ity proportional to $\langle \rho^2 \rangle_k(\omega)$ calculated using DSMC. c is the speed of sound. Finally, the training data set consists of total 40000 $(k, \omega, \langle \rho^2 \rangle)$ tuple. In the same way, we sample another 400 tuple as validation set.

The function M is modeled as a fully connected neural network as shown in 8. The weights to be trained is $\mathbf{W}_{1,2}$, notice that in our linear layer, the is no bias as usual. This is because we need to function to satisfy constraints as discussed in the paper. The weights are initialized using uniform initialization by as default

in Pytorch. We then compare the mean square difference between spectra $\langle \rho^2 \rangle_k(\omega)$ computed using DSMC with the spectra predicted by linear constitutive relation model. Using the loss in 9. The optimizer we use is the Adam optimizer with learning rate $\alpha = 0.005$, Beta parameter $\beta_1 = 0.9$ and $\beta_2 = 0.999$, and the parameter

$\epsilon = 10^{-8}$. For each training epoch, the batch size for each step is 64. The training process stops if the loss obtained on validation set increases. Since we are doing 1D function fitting using thousands of data, over-fitting is negligible, this is also tested by the velocity spectra predicted by our model.